A Comprehensive Approach to Roll-to-Roll Nanoimprinting Lithography

Juan P. Gomez-Constante[1], Prabhakar R. Pagilla[1], Kumbakonam R. Rajagopal[1]

[1]Texas A&M University, Department of Mechanical Engineering, College Station, Texas, United States of America

ABSTRACT

In this paper we present a novel mathematical model that replicates to some extent how general Roll-to-Roll Nano-Imprinting Lithography (R2RNIL) manufacturing processes work. We start by identifying some of the current challenges and problems that manufacturers face towards higher throughput and control of the manufacturing process. Next, we describe and analyze the main physical phenomena that constitute a typical R2RNIL process and the typical material properties of the polymers used as coatings and formulate a mathematical model that complies with the laws of Physics. We then present some numerical simulations that qualitatively reproduce several features that are found in experiments, under the linearizing assumptions employed to make the model amenable to numerical calculations. Furthermore, we identify some key process parameters and material properties affecting R2RNIL and how they can be useful for material design and process control. Finally, we will discuss future work and some applications that can be studied within the context of the general framework.

Keywords: multiphase multiscale modeling, viscoelastic material, photochemical bonding, mechanics of mixtures

NOMENCLATURE

ρ density of the mixture
ρ_i density of the constituent i (m: melt, s: solid)
ρ_{0i} initial density of the constituent i
$\boldsymbol{v}$ velocity of the mixture
$\boldsymbol{u}$ displacement of the mixture
t time
T_1 end time of the mold filling sub-process
T_2 end time of the phase change sub-process
T_3 end time of the demolding sub-process
$\boldsymbol{T}$ Cauchy stress tensor of the mixture
$\boldsymbol{T}_i$ Cauchy stress tensor of the constituent i
$\boldsymbol{L}$ velocity gradient of the mixture
$\boldsymbol{B}_{\kappa p_i(t)}$ Left Cauchy-Green tensor of the constituent i
G_i material constant of the constituent i
μ_i material constant of the constituent i
$\boldsymbol{b}$ body forces of the mixture
θ temperature of the mixture
$\boldsymbol{q}$ heat flux of the mixture
r radiant heating of the mixture
I light intensity of the mixture
σ_s absorbance of the mixture due to scattering
a_i absorption coefficient of the constituent i
c_i molecular concentration of the constituent i
M_i molecular weight of the constituent i
j_v radiation emitted by the mixture
N_A Avogadro's constant
h Planck's constant
v frequency of the photon
p Lagrange multiplier of isochoric assumption
$\boldsymbol{\tau}_i$ extra stress tensor of the constituent i
$\boldsymbol{\varepsilon}$ linearized strain tensor of the mixture
$\boldsymbol{\sigma}$ Cauchy stress tensor of the mixture associated to $\boldsymbol{\varepsilon}$
$\boldsymbol{I}$ Identity operator in $\mathbb{R}^3$
α mass fraction of the melt
λ_i stress-relaxation time of the constituent i
μ viscosity of the melt
G shear modulus of the solid
u_s displacement function of the substrate
I_0 light intensity of the UV-light source

1. INTRODUCTION

Roll-to-roll Nanoimprinting Lithography (R2RNIL) is a manufacturing process that enables high production volume and high geometric accuracy allowing mass-production of nano-scaled patterns, thus, lowering costs, increasing productivity, and accessibility of the technology. It has applications across many different fields such as automotive, electronic, chemical and aerospace industries. Despite all the current advances and applications, the physical process is still not well understood, and several persisting problems hinder future developments of this technology. Because of that, we propose a general framework that seeks to set a standard approach from which future mathematical models can be developed and modified. Among other things, this framework is capable of capturing the evolution of the pressure field (which most models cannot), predicting if a mold feature is going to be successfully filled or not, and predicting if an imprinted feature will be demolded correctly or damaged when demolding from the mold roller.

2. EXPERIMENTAL OBSERVATIONS

Experimental evidence suggests that the accuracy of the imprinted features decreases with increase in web speed.
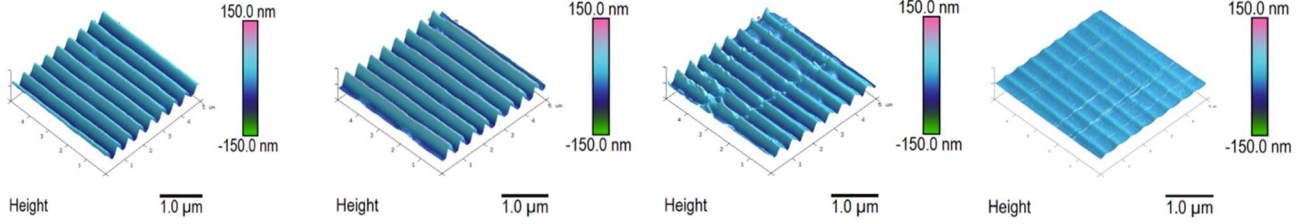
Figure 1: Characterization of imprinted patterns with imprint speeds (left to right) of 2, 5, 10, 20 m/min.

Figure 1 provides a characterization of the quality of imprinted patterns at different speeds[1]; notice that the period of the imprinted features is always the same whereas the height and overall quality of the feature decreases with increasing web speed. This suggests that there is an elastic-like behavior [1] that becomes more dominant as transport speed is increased. Another issue that is commonly reported is bubble formation in the imprinted features, which is also attributed to higher web speeds and pressures between rollers [2]. Additional factors like the geometry of the mold and the thickness of the coating film [3], as well as the high geometric aspect ratio [4] have been identified and analyzed. On the other hand, higher coating temperature is found to increase the accuracy of the imprinted features [5], a direct consequence of the more fluid-like material properties. A similar fluid-like behavior can be achieved by dissolving the coated polymer [6] in a fluid with better mechanical properties for mold filling. From the experimental behavior reported in the literature, it is evident that a better understanding of the physics behind the process and the web transport behavior could aid in improving throughput and quality of imprinted patterns.

3. PHYSICAL DESCRIPTION OF THE PROCESS

For the purpose of clearly depicting the R2RNIL process features, we identify the presence of three physical sub-processes in a typical R2RNIL process (Fig. 2), which are:

1. **Mold filling:** the coated substrate is pushed inside the mold cavities on the surface of a mold roller via the relative motion between the mold and nip rollers.
2. **Phase change:** the filled mold features are solidified by a change in temperature (thermal R2RNIL), ultraviolet (UV) curing (photochemical R2RNIL) or a combination of both.
3. **Demolding:** the solidified features on the substrate surface are debonded from the mold roller by employing a downstream demolding roller.
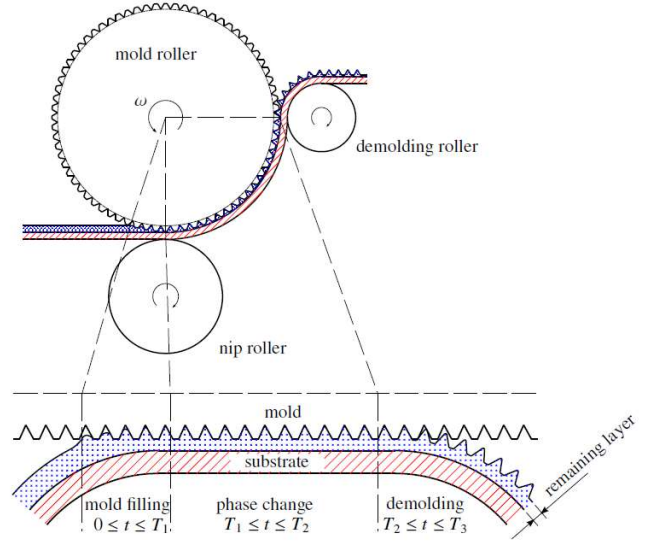
Figure 2: Illustration of the R2RNIL sub-processes and their time intervals.

4. PROPOSED FRAMEWORK

For the sake of simplicity of analysis, we will focus on one feature and follow it as it is transported through the three subprocesses. The R2R NIL process is governed by the balance equations:

$$\frac{d\rho}{dt} + \rho \operatorname{div} \boldsymbol{v} = 0 \tag{1}$$

$$\rho \frac{dv}{dt} = \operatorname{div} \boldsymbol{T} + \rho \boldsymbol{b} \tag{2}$$

$$\frac{du}{dt} = \boldsymbol{T} \cdot \boldsymbol{L} + \rho r + \operatorname{div} \boldsymbol{q} \tag{3}$$

$$\frac{dI}{dt} + c(\sigma_s + a_m c_m + a_s c_s)I = j_v + \frac{c}{4\pi}\int_\Gamma I \, da \tag{4}$$

where Eq. (1) is the conservation of mass, Eq. (2) is the conservation of linear momentum, Eq. (3) is the conservation of energy, and Eq. (4) is the equation governing the evolution of light intensity.

As for the polymeric fluids typically used as coatings, we model the fluid-solid mixture that coexists during the change of phase sub-process as a viscoelastic fluid and solid, respectively (see [7, 8, 9] for details). The viscous behavior of

---

[1] These experiments were conducted by Dr. Keith Good's research group and the imprinted patterns were measured by Dr. Don Lucca's research group, both at Oklahoma State University.

both constituents is characterized by a scalar rate of dissipation function due to mechanical working (ζ_i) whereas the elastic behavior is characterized by the Helmholtz potential (ψ_i). Both functions define a class of materials and can be experimentally determined. By considering the elastic behavior, we can determine how the energy stored in the form of internal stresses will affect the final outcome of the imprinted features. For the photochemical behavior we have taken the simplest type of reaction known in the literature as Photo-tunable Molecular Crosslinking (PMC) [10]. The constitutive equations that govern a typical R2R NIL process are given by:

$$T_m = G_m \frac{\rho_m \theta}{\rho_{0m} \theta_0} I + \frac{\rho_m}{\rho_{0m}} S_m \tag{5}$$

$$\frac{\mu_m}{G_m}\left(\frac{\theta_0}{\theta}\right) S_m^{\nabla} + \left[\frac{\rho_m}{\rho_{0m}} + \frac{\mu_m}{G_m}\frac{d}{dt}\left(\frac{\theta_0}{\theta}\right)\right] S_m$$
$$= 2\mu_m D + G_m \frac{\rho_m \theta}{\rho_{0m} \theta_0}\left(\frac{3}{\text{tr } B_{\kappa p_i(t)}} - 1\right) I \tag{6}$$

$$T_s = \frac{\rho_s}{\rho_{0s}} S_s \tag{7}$$

$$\frac{\mu_s}{G_{1s}} S_s^{\nabla} + \frac{\rho_s}{\rho_{0s}} S_s = G_{1s}\frac{\rho_s}{\rho_{0s}}\left(\frac{3}{\text{tr } B_{\kappa p_s(t)}} I + \frac{G_{2s}}{G_{1s}} B_{\kappa_r}\right) \tag{8}$$

$$\frac{\partial c_m}{\partial t} = -\frac{\epsilon}{N_A h\nu} c_m{}^2 I \tag{9}$$

where Eqs. (5) and (6) are the constitutive equations of the melt (fluid), Eqs. (7) and (8) are the constitutive equations of the solid, Eq. (9) is the particular photochemical reaction for a bimolecular polymer [10], and S^{∇} is the upper convected time derivative defined as

$$S^{\nabla} = \frac{d}{dt} S - LS - SL^T \tag{10}$$

The constitutive equations above are given in terms of either densities or molar concentrations only. The link between these thermomechanical-related densities and photochemical-related concentrations is given by the relation:

$$\rho_i = c_i M_i \tag{11}$$

4.1 Initial and Boundary Conditions

Balance laws and constitutive equations alone are not enough to model the R2R NIL process since initial and boundary conditions are also needed to complete the model. In our model, we consider that every sub-process has its own dominant physical phenomena, thus, making the definition of initial and boundary conditions time-dependent and their definition being given according to the sub-process. This identification of different initial and boundary conditions was done with the main purpose of isolating the information about each sub-process, and determine how each sub-process affects the overall R2R NIL process.

Table 1: Summary of R2R NIL sub-processes and their properties.

	mold filling	phase change	demolding
time interval	$0 \leq t \leq T_1$	$T_1 \leq t \leq T_2$	$T_2 \leq t \leq T_3$
phase	fluid	fluid & solid	solid
dominant phenomena	mechanical deformation	temperature / UV curing	mechanical deformation
initial conditions	$\rho(x,0) = \rho_{0m}$ $u(x,0) = 0$ $v(x,0) = 0$ $T(x,0) = 0$ $I(x,0) = 0$ $\theta(x,0) = \theta_0$	$\rho(x,T_1)$ $u(x,T_1)$ $v(x,T_1)$ $T(x,T_1)$ $I(x,T_1)$ $\theta(x,T_1)$	$\rho(x,T_2)$ $u(x,T_2)$ $v(x,T_2)$ $T(x,T_2)$ $I(x,T_2)$ $\theta(x,T_2)$
main boundary condition	$u_s(t)$	I_0, θ_a	$u_s(t)$
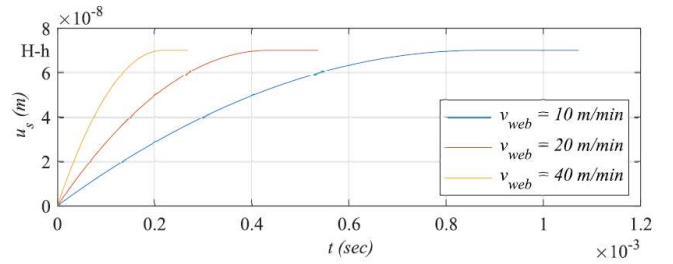
Figure 3: Evolution of substrate displacement $u_s(t)$ during mold filling ($0 \leq t \leq T_1$) for different web speeds.
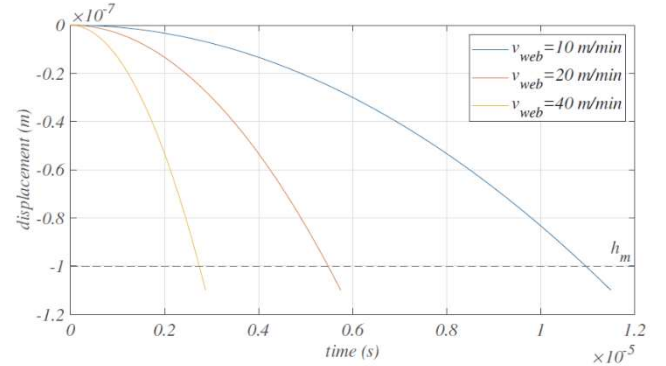
Figure 4: Evolution of substrate displacement $u_s(t)$ during demolding ($T_2 \leq t \leq T_3$) for different web speeds with a mold feature of height $h_m = 100\ nm$ and width $b_m = 300\ nm$.

We identified the substrate boundary conditions as the driving forces of each sub-process since they carry the main information of source of energy for each sub-process. For both the mold filling and demolding sub-processes, transport under tension and nip forces are employed to achieve the displacement of the substrate $u_s(t)$ (Figs. 3 and 4 respectively) whereas the intensity of the UV light source or the heat convection from a heated mold roller governs the phase change process (Fig. 5).
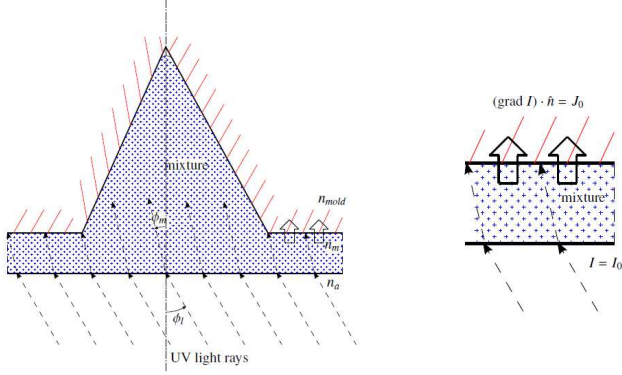
Figure 5: UV light incidence angle on a single mold feature (left). The incidence angle changes from ϕ_l in air to ϕ_m in mixture. Boundary conditions of the intensity of light I at the boundaries (right).

4.2 Linearized Problem

Solving the general model, even numerically, is a difficult task, and one has to make several simplifying assumptions which help in reducing some of the numerical issues. Assuming that the gradient of the displacement, strain and strain rate are small, the body forces can be neglected, mixture undergoes isochoric motion, the temperature is uniform and does not vary with time, and the density of the mixture is uniform in space and time, we can combine the balance equations with the constitutive equations and obtain the following simplified governing equations:

$$\text{div}\left(\frac{\partial \boldsymbol{u}}{\partial t}\right) = 0 \tag{12}$$

$$\rho \frac{\partial^2 \boldsymbol{u}}{\partial t^2} = -\frac{\partial p}{\partial x} + \frac{\mu}{\lambda_1}\frac{\partial \alpha}{\partial x} + \text{div}(\alpha\boldsymbol{\tau}_m + (1-\alpha)\boldsymbol{\tau}_s) \tag{13}$$

$$\frac{\partial I}{\partial t} + \hat{r} \cdot \frac{\partial I}{\partial x} + \left[\frac{a_m\rho}{M_m}\alpha + \frac{a_s\rho}{M_s}(1-\alpha)\right]I = 0 \tag{14}$$

where the evolution of $\boldsymbol{\tau}_m$, $\boldsymbol{\tau}_s$ and α are defined as

$$\lambda_1 \frac{\partial \boldsymbol{\tau}_m}{\partial t} + \alpha\boldsymbol{\tau}_m = 2\mu\frac{\partial \boldsymbol{\varepsilon}}{\partial t} \tag{15}$$

$$\lambda_2 \frac{\partial \boldsymbol{\tau}_s}{\partial t} + (1-\alpha)\boldsymbol{\tau}_s = 2(1-\alpha)G\boldsymbol{\varepsilon} \tag{16}$$

$$\frac{\partial \alpha}{\partial t} = -\frac{\epsilon\rho}{M_m N_A h\nu}\alpha^2 I \tag{17}$$

5. RESULTS AND DISCUSSION

Using an even more simplified 2D-model based on the linearized version of the problem and using a finite difference method suitable for free boundary calculations [11], a numerical scheme was implemented in MATLAB®. The numerical analysis of results is divided into two categories: the effects of the transport and process parameters defining R2R NIL and the effects of the material properties of the coating film.

5.1 Effect of Process Parameters

Numerical simulations indicated that the overall filling accuracy decreases with the increase in the web transport speed, which is consistent with the experimental observations. Numerical results also indicate that the linearized model is general enough to be scale-sensitive, that is, if we increase the geometric scale of the mold feature, but keeping the same aspect ratio, the overall mold filling behavior changes as depicted in Figure 6.
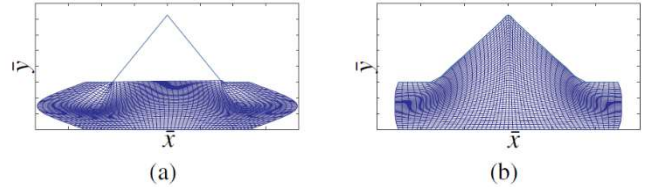
Figure 6: Effect of imprint feature geometric scale in the linearized model. In (a) stress-relaxation time and surface tension play a major role in preventing mold filling, but these effects disappear with the increase in both H and L by a factor of 10 as shown in (b).

Figure 7 shows two different scenarios of the phase change process for two different types of boundary conditions: (1) traction-force only and (2) stationary-substrate only. In the top left figure, the mixture starts as a melt at rest (beginning of mold filling), and then the substrate (lower boundary) moves up causing the mold cavity to be completely filled if the material and process parameters are adequate (top right) which also determines the initial state of the phase change sub-process (at time $t = T_1$). If the traction-force only boundary conditions are enforced then the fluid film recoils back stretching on the sides and shrinking in the center (bottom left). If the stationary-substrate only boundary conditions are enforced, then the energy is dissipated (bottom right). The recoiling observed in the traction-force boundary conditions make the values of p (Lagrange multiplier) several orders of magnitude smaller than the ones observed with the stationary-substrate boundary conditions.
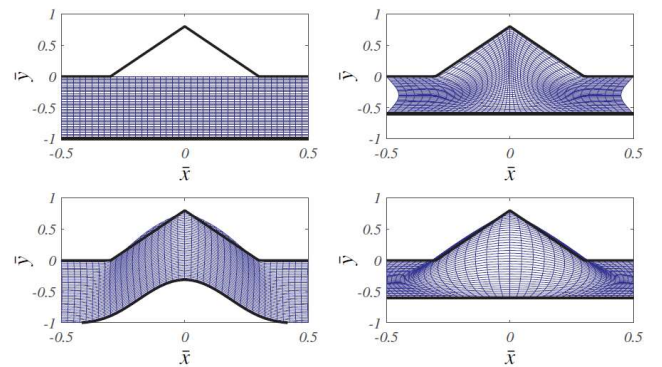
Figure 7: Mixture film (blue fiber mesh) and mold/substrate boundaries (solid black lines) on mold filling and phase change processes for one feature.

Figure 8 provides the L^2-norm of the extra stress, strain and Lagrange multiplier that enforces the isochoric motion assumption of the mixture and the mass fraction of the melt as they evolve in nondimensional time at two different web speeds (10 m/min and 40 m/min) for both boundary condition scenarios. In the extra stress of the mixture ($\boldsymbol{\tau} = \boldsymbol{\tau}_m + \boldsymbol{\tau}_s$) (top left of Figure 8) we can observe a sudden jump at the beginning of the phase change process consistent with the instantaneous mold filling process at both web speeds to then relax to lower values for both boundary conditions. Notice that 40 m/min web speed resulted in higher initial stress. With higher initial stress values and higher web speed, the energy stored in the mixture does not have adequate time to for dissipation as in the case of the 10 m/min web speed curves. In the linearized strain of the mixture ($\boldsymbol{\varepsilon} = \boldsymbol{\varepsilon}_m = \boldsymbol{\varepsilon}_s$) (top right subfigure of Figure 8), we again observe a sudden jump during the mold filling sub-process, however, only this time, the initial strain is the same regardless of the web speed. Notice that at 40 m/min the time available for phase change is small enough that the strain remains approximately constant, whereas at 10 m/min the strain has adequate time to relax. As for the Lagrange multiplier term (bottom left of Figure 8), we observe a sudden jump again which subsequently reaches a value that is the same regardless of the web speed. The two scenarios (expressed as different boundary conditions) produce values that are several orders of magnitude different. Finally, in the mass fraction of the melt (bottom right of Figure 8), we observe that the two different scenarios play no role in the amount of melt being converted into solid. In addition, we also observe that higher web speeds produce lower time rates of phase change and therefore a smaller amount of melt being converted into solid at the end of the phase change sub-process.
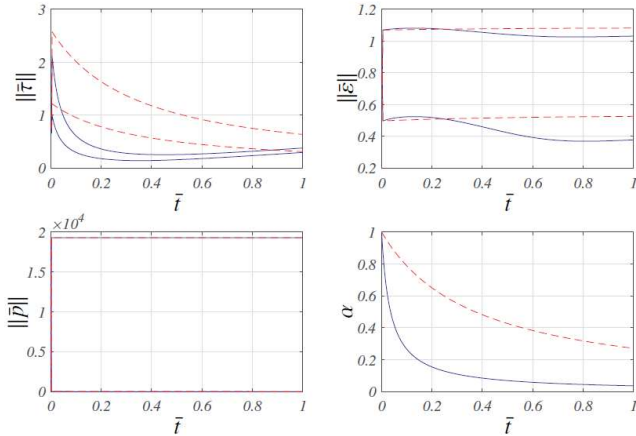
Figure 8: L^2-norm of extra stress, strain, pressure, and mass fraction of the melt at 10 m/min (solid blue) and 40 m/min (dashed red). The two different curves at the same web speed identify the stationary-substrate (higher value) and traction-force (lower value) boundary conditions.

Figure 9 depicts the normal component of the Cauchy stress of the mixture ($\boldsymbol{\sigma} = -p\boldsymbol{I} + \boldsymbol{\tau}$) acting on the upper (mold-mixture) and lower (mixture-substrate) boundaries during the demolding sub-process. We trace the evolution of both boundaries as a single point since the extra stress tensor terms are several orders of magnitude smaller than the Lagrange multiplier term of the stress which is approximately uniform across the spatial domain, so its evolution is mainly perceived in time. From the figure it is evident that higher web speeds produce higher tensile normal stresses at the end of the demolding sub-process. The periodic fluctuation we observe at the beginning of the process is mainly due to the numerical instabilities related to the numerical method used for the simulations and this effect becomes stronger with higher web speeds.
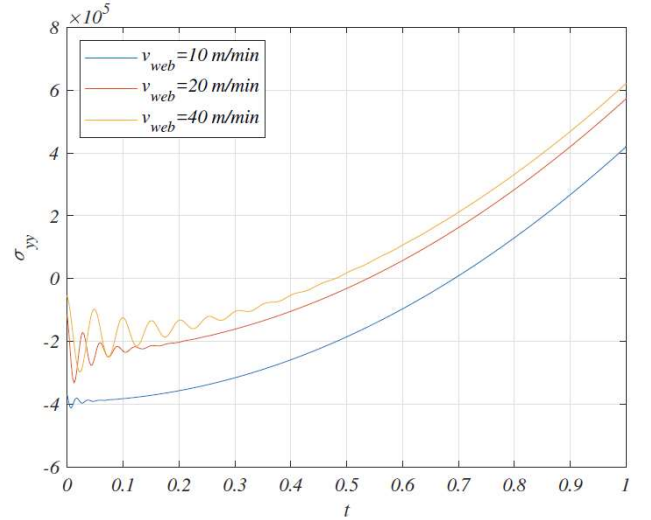
Figure 9: Non-dimensional normal stress and its evolution in the demolding sub-process.

5.2 Effect of Material Properties

Figure 10 shows some numerical simulations by considering the key material properties affecting mold filling, namely stress-relaxation time, surface tension and viscosity. The lack of smoothness in the curves is caused by error accumulation arising from the numerical instability inherent to the numerical method. From the plots we observe that higher the values of stress-relaxation time and surface tension result in lower percentages of mold filling. It is also worth observing that contrary to the general thought process in the reported literature, higher film viscosities lead to better mold filling. This observation is consistent with the fact that for higher values of viscosity, the material dissipates more energy therefore less energy is available for recoiling to a previous state.
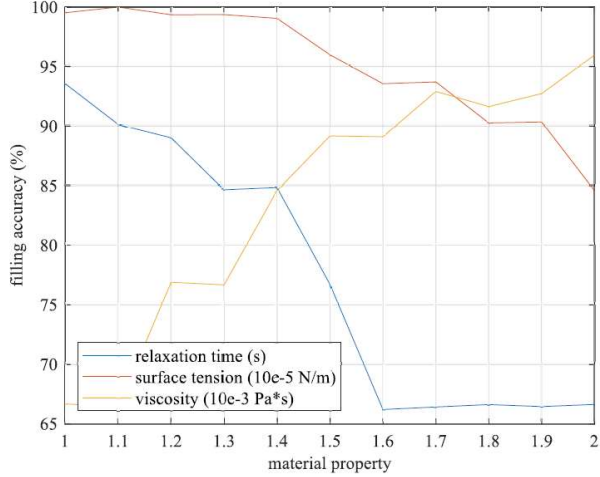
Figure 10: Filling accuracy as function of the stress-relaxation time, surface tension and viscosity at a web speed of 40 m/min.

As for the normal forces acting on the upper and lower boundaries during demolding (Figure 11), we observe that the values of the normal force are somewhat similar, for various values of alpha-parameter, regardless of the portion of the melt in the mixture. However, notice that a lower proportion of melt (or higher the proportion of solid) in the mixture produces a slightly lower normal tensile force at the end of demolding. As in the previous demolding plot (Figure 10), the fluctuations are mainly due to numerical instabilities getting stronger with higher proportion of solid.
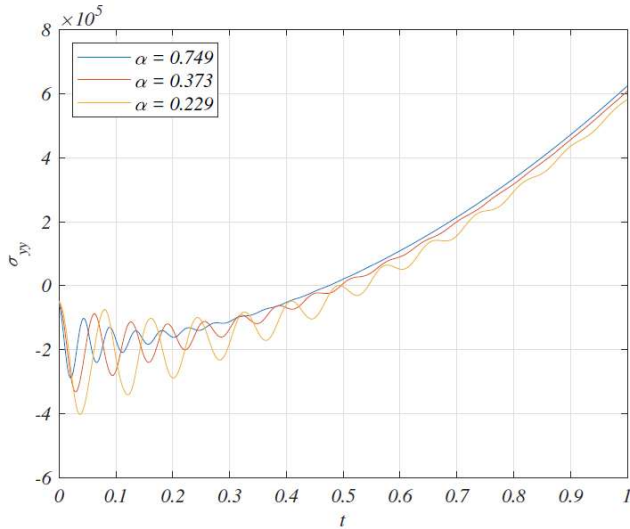
Figure 11: Non-dimensional normal stress and its evolution for different fractions of melt in the demolding sub-process.

Although numerical results reproduce several phenomena observed in experiments, one must use caution in interpreting these results quantitatively since linearizing assumptions could potentially lead to incorrect observations from the quantitative viewpoint; a well-designed set of experiments must be conducted to support these numerical observations, both qualitatively and quantitatively.

6. CONCLUSIONS AND FUTURE WORK

As we have seen from numerical simulations, if we increase the web speed, then the elastic-like behavior is more dominant across all the three sub-processes. Increased transport speeds produce lower accuracy of mold filling and lower proportion of solidification in phase change, but a higher tensile normal stress on the boundaries which means an easier pathway to successfully demold the imprinted web provided that the normal tensile stresses are smaller than the yield strength of the coating material and higher than the adhesive stresses on the mold-roller/mixture interface. It is also important to mention that the smaller the scale of the imprinted patterns, the higher the elastic-like behavior of the coated film, thus a lower mold filling accuracy.

From the material properties point of view, we see that it is desirable to have coating materials with smaller values of stress-relaxation time and surface tension since they are beneficial for mold filling. On the other hand, and contrary to what is reported in the literature, it is desirable to have coating film materials with higher viscosity since this property enhances mold filling accuracy.

It is also worth noting that even a linearized version of the general framework that we have proposed is capable of qualitatively replicating key observations from existing R2RNIL experimental data. With the general framework in place, we only need to characterize the coating film material via the rate of dissipation due to mechanical working (ζ) and the Helmholtz potential (ψ) with relatively simple experiments.

Table 2: Summary of observations

increase in	mold filling	phase change	demolding
web speed	lower accuracy	lower solidification	better debonding
web tension	N/A	higher internal stresses	N/A
UV-light intensity	N/A	higher solidification	N/A
Viscosity	higher accuracy	lower internal stresses	N/A
relaxation time	lower accuracy	N/A	N/A
surface tension	lower accuracy	N/A	N/A

A next step towards the completion of this general framework is a more detailed analysis of the demolding sub-process. Initial simulations concerning this work suggest a dependence between the web speed and cohesive/adhesive failure. However, one of the key challenges is the accumulation of error due to the elastic behavior and the propagation of error due to the nature of the numerical method used for calculations.

We can also investigate more realistic boundary conditions (such as stick-slip boundary conditions which are more amenable for polymers), relax some (or all) of the linearizing assumptions to allow for large deformations, and investigate coating materials with a more complex thermomechanical or photo-chemical behavior. In addition, we plan to incorporate temperature changes to the model due to the highly exothermic photo-chemical process that takes place during phase change and the fact that most of the energy irradiated by the UV light source is absorbed by the mold roller and dissipated to the surroundings.

ACKNOWLEDGMENTS

REFERENCES

[1] Horiba, M. Yasuda, H. Kawata, M. Okada, S. Matsui, Y. Hirai, Impact of resist shrinkage and its correction in nanoimprint lithography, Japanese Journal of Applied Physics 51 (6S) (2012) 06FJ06.

[2] H. Wu, P. Yi, L. Peng, X. Lai, Study on bubble defects in roll-to-roll uv imprinting process for micropyramid arrays. i. experiments, Journal of Vacuum Science & Technology B, Nanotechnology and Microelectronics: Materials, Processing, Measurement, and Phenomena 34 (2) (2016) 021201.

[3] C.-H. Lin, R. Chen, Impacts of mold geometries and imprinted resist thickness on velocity fields for nanoimprint lithography, Japanese Journal of Applied Physics 47 (6S) (2008) 5197.

[4] M. Matschuk, N. B. Larsen, Injection molding of high aspect ratio sub-100 nm nanostructures, Journal of Micromechanics and Microengineering 23 (2) (2012) 025003.

[5] K.-J. Sohn, J. H. Park, D.-E. Lee, H.-I. Jang, W. I. Lee, Effects of the process temperature and rolling speed on the thermal roll-to-roll imprint lithography of flexible polycarbonate film, Journal of Micromechanics and Microengineering 23 (3) (2013) 035024.

[6] S.-H. Lee, H.-N. Kim, R.-K. Kwak, K. Y. Suh, Effects of mold rising angle and polymer concentration in solvent-assisted molding, Langmuir 25 (20) (2009) 12024–12029.

[7] J. P. Gomez-Constante, P. R. Pagilla, K. R. Rajagopal, Effect of the processing and transport parameters on mold filling in roll-to-roll nanoimprint lithography, in: Proceedings of the Fifteenth International Conference on Web Handling, 2019.

[8] J. P. Gomez-Constante, P. R. Pagilla, K. R. Rajagopal, A thermomechanical description of the mold filling process in roll-to-roll nanoimprinting lithography, Applications in Engineering Science 1 (1) (2020) 100001.

[9] J. P. Gomez-Constante, P. R. Pagilla, K. R. Rajagopal, A thermomechanical and photochemical description of the phase change process in roll-to-roll nanoimprinting lithography, International Journal of Engineering Science 169 (2021) 103564.

[10] K. N. Long, T. F. Scott, H. J. Qi, C. N. Bowman, M. L. Dunn, Photomechanics of light-activated polymers, Journal of the Mechanics and Physics of Solids 57 (7) (2009) 1103–1121.

[11] F. H. Harlow, J. E. Welch, Numerical calculation of time-dependent viscous incompressible flow of fluid with free surface, The physics of fluids 8 (12) (1965) 2182–2189.